Environmental controls on sediment grain properties of Peruvian coastal river basins

Camille Litty[1], Fritz Schlunegger[1], Willem Viveen[2]

[1] *Institute of Geological Sciences, University of Bern, Baltzerstrasse 1+3, CH- 3012 Bern.*

[2] *Sección de Ingeniería de Minas e Ingeniería Geológica, Departamento de Ciencias e Ingeniería, Pontificia Universidad Católica del Perú, San Miguel, Lima, Perú.*

ABSTRACT

Twenty-one coastal rivers located on the western Peruvian margin were analyzed to determine the relationships between fluvial and tectonic processes and sediment grain properties. Modern gravel beds were sampled along a north-south transect on the western side of the Peruvian Andes where the rivers cross the tip of the mountain range, and at each site the long *a*-axis and the intermediate *b*-axis of about 500 pebbles were measured. Morphometric properties of each drainage basin were determined and compared against measured grain properties. Grain size data show a large scatter in the D_{50}, D_{84}, D_{96} values and in the ratio between the intermediate and the long axis. We have not found any correlations between the frequency of earthquakes and the grain size pattern, which suggests that the current seismic, and likewise tectonic, regime has no major controls on the supply of material on the hillslopes and the grain size pattern in the trunk stream. However, positive correlations between water shear stresses, mean basin denudation rates, mean basin slopes and basin sizes on nearly all grain size percentiles suggest a geomorphic control where larger denudation rates operating in larger basins, and steeper basins, paired with

larger flow shear stresses, are capable of transporting more and coarser grained material. Furthermore, we use correlations between the clasts' sphericities and transport distances to infer a transport time control on the shape of the clasts. We thus suggest that the grain size distribution of gravel bars and the fabric of individual clasts has dynamically adjusted to water and sediment flux and their specific time scales.

1. INTRODUCTION

The size and shape of gravels bear crucial information about (i) the transport dynamics of mountain rivers (Hjulström, 1935; Shields, 1936; Blissenbach, 1952; Koiter et al., 2013; Whittaker et al., 2007; Duller et al., 2012; Attal et al., 2015), (ii) the mechanisms of sediment supply and provenance (Parker, 1991; Paola et al., 1992a, b; Attal and Lavé, 2006), and (iii) environmental conditions such as uplift and precipitation (Heller and Paola, 1992; Robinson and Slingerland, 1998; Foreman et al., 2012; Allen et al., 2013; Foreman, 2014). The mechanisms by which grain size and shape change from source to sink have often been studied with flume experiments (e.g. McLaren and Bowles, 1985; Lisle et al., 1993) and numerical models (Hoey and Ferguson, 1994). These studies have mainly been directed towards exploring the controls on the downstream reduction in grain size of gravel beds (Schumm and Stevens, 1973; Hoey and Fergusson, 1994; Surian, 2002; Fedele and Paola, 2007; Allen et al., 2016). In addition, it has been proposed that the grain size distribution particularly of mountainous rivers reflect the erosional processes at work on the bordering hillslopes. This has recently been illustrated based on a study encompassing all major rivers in the Swiss Alps with sources in various litho-teconic units of the Central European Alps (Litty and Schlunegger, 2017). Among the various processes, the supply of material through landsliding (van den Berg and Schlunegger, 2012) and torrential floods in tributary rivers (Bekaddour et al., 2013) were proposed to have the greatest influence on the grain size distribution in these rivers (Allen et al., 2013), where tributary pulses of sediment supply alter the caliber of the trunk stream material. Accordingly, the nature of erosional processes on valley flanks are likely to have a measurable impact on the supply of material to the valleys' trunk rivers, and thus on the sediment caliber in these streams.

Among the various conditions, hillslope erosion and the supply of material to the trunk stream has been shown to mainly depend on: (i) tectonic uplift resulting in steepening of the entire landscape (Dadson et al., 2003; Wittmann et al., 2007; Ouimet et al., 2009), (ii) earthquakes and seismicity causing the release of large volumes of landslides (Dadson et al., 2003; McPhillips et al., 2014), (iii) precipitation rates and patterns, controlling the streams' runoff and shear stresses (Litty et al., 2017), and (iv) bedrock lithology where low erodibilty lithologies are sources of larger volumes of material (Korup and Schlunegger, 2009). Because most of the bedload material of rivers has been derived from hillslopes bordering these rivers, as mapping and grain size analyses of modern rivers in the Swiss Alps have shown (Bekaddour et al., 2014; Litty and Schlunegger, 2017), it is very possible that the grain size distribution of modern rivers either reflect the seismic processes at work, or rather reveal the response to the climate conditions such as rainfall rates and the shear stresses of rivers.

The western margin of the Peruvian Andes represents a prime example where these mechanisms and related controls on the grain size distribution of river sediments can be explored. In particular, this mountain belt experiences intense and frequent earthquakes (Nocquet et al., 2014) in response to subduction of the oceanic Nazca plate beneath the continental South American plate at least since late Jurassic times (Isacks, 1988). Therefore, it is not surprising that erosion and the transfer of material from the hillslopes to the rivers has been considered to strongly depend on the occurrence of earthquakes, as measured ^{10}Be concentrations in pebbles suggest (McPhilipps et al., 2014). On the other hand, it has also been proposed that denudation in this part of the Andes is controlled by the distinct N-S and E-W precipitation rate gradients. These inferences have been made based on concentrations of in-situ cosmogenic ^{10}Be measured in river-born quartz (Abbühl et al., 2011; Carretier et al., 2015; Reber et al.,in press), and on morphometric analyses of the western Andean landscape (Montgomery et al., 2001). Because erosion has been related to either the occurrence of earthquakes and thus to tectonic processes (McPhillips et al., 2014) or rainfall rates (Abbühl et al., 2011; Carretier et al., 2015) and thus to the stream's mean annual runoff (Reber et al., in press), and since hillslope erosion and the supply of material to trunk streams is likely to influence, or at least to perturb, the caliber of the bedload material in mountainous streams (Bekaddour et al., 2013), it is possible that the grain size pattern in Peruvian trunk rivers reflects the ensemble of these mechanisms at work.

Here we present data on sediment grain properties from rivers situated on the western margin of the Peruvian Andes (Figure 1A) in order to elucidate the possible effects of intrinsic factors such as morphometric properties of the drainage basins, and extrinsic properties (runoff and seismic activity) on sediment grain properties. To this extent, we collected grain size data from gravel bars of each stream along the entire western Andean margin of Peru that are derived from 21, over 700-km^2-large basins. Sampling sites were situated at the outlets of valleys close to the Pacific Coast.

1.1 Geologic and tectonic setting

The study area is located at the transition from the Peruvian Andes to the coastal lowlands along a transect from the cities of Trujillo in the north (8°S) to Tacna in the south (18°S). In northern and central Peru, a flat, up-to 100 km, broad coastal forearc plain with Paleogene-Neogene and Quaternary sediments connects to the western Cordillera. This part of the western Cordillera consists of Cretaceous to late Miocene plutons of various compositions (diorite, but also tonalite, granite and granodiorite) that crop out over an almost continuous 1600-km long arc that is referred to as the Coastal Batholith (e.g. Atherton, 1984; Mukasa, 1986; Haederle and Atherton, 2002; Figure 1B). In southern Peru, the coastal plain gives way to the Coastal Cordillera that extends far into Chile. The western Cordillera comprises the central volcanic arc region of the Peruvian Andes with altitudes of up to 6768 m.asl, where currently active volcanoes south of 14°S of latitude are related to a steep slab subduction. On the other hand, Cenozoic volcanoes in the central and northern Peruvian arc have been extinct since c. 11 Ma due to a flat slab subduction, which inhibited magma upwelling from the asthenosphere (Ramos, 2010).

The bedrock of the Western Cordillera is dominated by Paleogene, Neogene and Quaternary volcanic rocks (mainly andesitic or dacitic tuffs, and ignimbrites) originating from distinct phases of Cenozoic volcanic activity (Vidal, 1993). These rocks rest on Mesozoic and Early Tertiary sedimentary rocks (Figure 1B).

The local relief along the western Cordillera has been formed by deeply incising rivers that flow perpendicular to the strike of the Andes (Schildgen et al., 2007). The morphology of the longitudinal stream profiles is characterized by two segments separated by a distinct knickzone (Trauerstein et al., 2013). These geomorphic features have formed through headward retreat in response to a phase of enhanced surface uplift during the late Miocene (e.g., Schildgen et al., 2007). Upstream of these knickzones, the streams are mainly underlain by Tertiary volcanoclastic rocks, while farther downstream incision has disclosed the Coastal Batholith and older meta-sedimentary units (Trauerstein et al. 2013). The upstream edges of these knickzones also delineate the upper boundaries of the major sediment sources (Litty et al., 2017). In contrast, little to nearly zero clastic material has been derived from the headwater reaches in the Altiplano, where the flat landscape has experienced nearly zero erosion, as 10Be-based denudation rate estimates (Abbühl et al., 2011) and provenance tracing have shown (Litty et al., 2017).

The tectonic conditions of the western Andean are characterized by strong N-S gradients in Quaternary uplift, seismicity and long-term subduction processes. In particular, the coastal segment south of 13°S and particularly south of 16°S hosts raised Quaternary marine terraces (Regard et al., 2010), suggesting the occurrence of surface uplift at least during Quaternary times. This is also the segment of the Andes where the Nazca plate subducts at a steep angle and where the current seismicity implies a relatively high degree of interseismic coupling, resulting in a high frequency of earthquakes with magnitudes M>4 (Nocquet et al., 2014). In contrast, the northern segment of the coastal Peruvian margin hosts a coastal plain that has been subsiding (Hampel, 2002). Also in this region, the interseismic coupling along the plate interface is low, as revealed by the relatively low frequency of earthquake occurrence (Nocquet et al., 2014).

1.2 Climatic setting

The N-S-oriented, annual rainfall rates decrease from 1000 mm per year near the Equator to 0 mm along the coast in southern Peru and northern Chile (Huffman et al., 2007; Figure 1C). The Peruvian western margin shows an E-W contrasting precipitation pattern with high annual precipitation rates up to 800 mm on the Altiplano and c. 0 mm per year on the coast (Figure 1C). This precipitation gradient in the western Andes is related to the position of the Intertropical Convergence Zone (ITCZ, inset of Figure 1C) associated with an orographic effect on the eastern side of the Andes (Bookhagen and Strecker, 2008). During austral summer (January) the center of the ITCZ is located farther south, transferring the moisture from the Amazon tropical basin to the Altiplano (Garreaud et al., 2009) and leading to a wet climate on the Altiplano with strong precipitation rates. During austral winter, the Altiplano is under the influence of dry air masses from the subsiding branch of the Hadley cell that result in a more equatorial position of the ITCZ and in a dry persistent westerly wind with almost no precipitation on the Altiplano. Additionally, the Andes form an orogenic barrier preventing Atlantic winds and moisture to reach the coast. Only in northern Peru around 5°S latitude, the ocean water sufficiently warms up because of the mixing with the tropical current derived from Ecuador, resulting in precipitation in northern Peru. In addition, every 2 to 10 years, near to the Equator, the Pacific coast is subjected to strong precipitation resulting in high flood variability, related to the El Nino weather phenomenon (ENSO) (DeVries, 1987).

2. SITE SELECTION AND METHODS

We selected river basins between 8°S and 18°S latitude situated on the western margin of the Peruvian Andes, because of the presence of marked N-S contrasts in precipitation rates and the presence of strong seismic activity due to the subduction of the Nazca plate (Table 1). Only the main river basins were selected, which were generally larger than 700 km^2. These basins have recently been analyzed for ^{10}Be-based catchment averaged denudation rates and mean annual water fluxes (Reber et al., in press). This allows us to explore whether sediment flux, which equals the product between ^{10}Be-based denudation rates and basin size, has a measurable impact on the grain size pattern. In addition, also for these streams, Reber et al. (in press) presented data on mean annual water discharge using the records of gauging stations and the TRMM-

V6.3B43.2 precipitation dataset as basis (Huffman et al., 2007). We will use this information to explore the controls of water shear stresses on the caliber of the bedload material (see below).

Sampling sites were situated in the main river valleys in the western Cordillera just before it gives way to the coastal margin. We selected the downstream end of these rivers because the grain size pattern at these sites is likely to record the ensemble of the main conditions and forces controlling the supply of material to the trunk stream farther upstream. We randomly selected c. five longitudinal bars where we collected our grain size dataset. Sampling sites are all accessible along the Pan-American Highway (see Table 1 for the coordinates of the sampling sites). Additionally, the Majes basin (marked with red color on Figure 1A), which is part of the 21 studied basins, has been sampled at five sites from upstream to downstream to explore the effects related to the sediment transport processes for a section across the mountain belt, but along stream (Figure 2; Table 2). The Majes basin has been chosen because of its easy accessibility in the upstream direction and because the morphology of this basin has been analyzed in a previous study (Steffen et al., 2010).

It has been shown that using a standard frame with fixed dimensions to assist gravel sampling reduces user-biased selections of gravels (Marcus et al., 1995; Bunte and Abt, 2001a). In order to reduce this bias, we substituted the frame by shooting an equal number of photos at a fixed distance (c. 1 m) from the ground surface at each longitudinal bar. Ten photos were taken from an approximately 10 m^2-large area to take potential spatial variabilities among the gravel bars into account. From those photos, the intermediate *b*-axes and the ratio of the *b*-axes and the long *a*-axis of around 500 randomly chosen pebbles were manually measured (Bunte and Abt, 2001b) and processed using the software program ImageJ (Rasband, 1997). Our sample population exceeds the minimum number of samples needed for statistically reliable estimations of grain size distributions in gravel bars (Howard, 1993; Rice and Church, 1998).

The pebbles were characterized on the basis of their median (D_{50}), the D_{84} and the coarse (D_{96}) fractions. This means that 50%, 84% and 96% of the sampled fraction is finer grained than the 50^{th}, 84^{th} and 96^{th} percentile of the samples. On a gravel bar, pebbles tend to lie with their short axis perpendicular to the surface, thus exposing their section that contains the *a*- and *b*-axes (Bunte and Abt, 2001b). However, the principal limitation is the inability to accurately measure the fine particles < 3 mm (see also Whittaker et al., 2010). While we cannot resolve this problem with the techniques available, we do not expect that this adds a substantial bias in the grain size distributions reported here as their relative contributions to the point-count results are minor (i.e. < 5%, based on visual inspection of the digital images).

Catchment-scale morphometric parameters and characteristics, including drainage area slope angle and slope at sampling site (Table 1), were extracted from the 90-m-resolution digital elevation model Shuttle Radar Topography Mission (SRTM; Reuter et al., 2007). The distances from the sample sites to the upper edge of the Western Escarpment (Trauerstein et al., 2013) have been measured.

Because grain size patterns largely depend on water shear stresses, we explored where such correlations exist for the Peruvian rivers. We thus computed water shear stresses τ following by Hancock and Anderson (2002) and Litty et al. (2016), where:

$$\tau = 0.54pg\left(\frac{Q}{W}\right)^{0.55} S^{0.93} \qquad (1).$$

Here, $\rho=1000\ kg/m^3$ is the water density, g the gravitational acceleration, Q (m^3/s) is mean annual water discharge that we have taken from Reber et al. (in press), W (m) the channel width, and S (*m/m*) is the channel gradient. Channel gradients at the sampling sites were calculated using the 90-m-resolution DEM as a basis. In addition, stream channel widths at each sampling site and at the time of the sampling campaign (May 2015) were measured on satellite images when available, and on field images with uncertainties of about 2 m. In addition, we have considered the basin mean denudation rates (Reber et al., in press; Table 1) as variable because larger denudation rates points towards a larger relative sediment flux, which in turn could influence downstream fining rates of grain sizes (Dingle et al., 2017).

Possible covariations and correlations between grain size and/or morphometric parameters and basin characteristics were evaluated using Pearson correlation coefficients; thus providing corresponding r-values (Table 3) and p-values with a significance level alpha < 0.1 (Table 4). The r-values measure the linear correlations between variables. The values range between +1 and −1, where +1 reflects a 100% positive linear correlation, 0 reflects no linear correlation, and −1 indicates a 100% negative linear correlation (Pearson, 1895). Threshold values of > + 0.30 and < - 0.30 were selected to assign positive and negative correlations, respectively.

3. RESULTS

3.1 Grain size

The results of the grain size measurements reveal a large variation for the *b*-axis where the values of the D_{50} range from 1.3 cm to 5.5 cm for rivers along the entire western Peruvian margin (Figure 3h; Table 1). Likewise, D_{84} values vary between 3 cm and 10.5 cm. The sizes for the D_{96} reveal the largest spread, ranging from 6 cm to 31 cm. In addition, the ratio between the lengths of the *b*-axis and *a*-axis (sphericity ratio) varies between 0.67 and 0.74 (Figure 3i). Note that between 15.6°S and 13.7°S, no gravel bars are encountered in the rivers where they leave the mountain range, and only sand bars can be found. Therefore no results are exhibited for these latitudes (Figure 3h and 3i).

3.2 The Majes basin

The D_{50} percentile of the *b*-axis decreases from 6.2 cm at 106 km river upstream to a value of 5.2 cm at 20 km upstream for the Pacific coast (Figures 2 and 4 and Table 2). Likewise, the D_{84} decreases from 19 cm to 8.7 cm, and the D_{96} decreases from 31 cm to 11.6 cm (Figure 4). Geomorphologists widely accept the notion that the downstream hydraulic geometry of alluvial channels reflects the decrease of particle size within an equilibrated system involving stream flow, channel gradient, sediment supply and transport (e.g. Hoey and Ferguson, 1994; Fedele and Paola, 2007; Attal and Lavé, 2009). Sternberg (1875) formalized these relations and predicted an exponential decline in particle size in gravel bed rivers as a consequence of abrasion and selective transport where the gravel is transported downstream. The relation follows the form: $D_x = D_0\, e^{-\alpha x}$ (Sternberg, 1875). Here, the exponent α decreases from 0.3 for the largest percentile (i.e., the D_{96}) to c. 0.1 for the D_{50} (Figure 4).

3.3 Correlations between grain sizes and morphometric properties

Table 3 shows the Pearson correlation coefficients (r-value) between the grain sizes, the morphometric parameters and the characteristics of the basins. As was expected, the D_{50}, D_{84} and D_{96} all strongly correlate with each other (0.73 < r-value < 0.93), but the *b/a* ratios do not correlate with any of the 3 percentiles (-0.1 < r-value < 0.1). The D_{50} values positively (but weakly) correlate with the sizes of the catchment area (r-value = 0.31), the distances from the Western Escarpment (r-value = 0.35), the mean annual shear stress at the sampling site (r-value =

0.23), the denudation rates (r-value = 0.34) and the sediment fluxes (r-value = 0.42; Figure 5A).The sediment fluxes show the highest significance level; p-value = 0.05 (Table 4). The D_{84} and the D_{96} values correlate positively with the shear stress exerted by the water on an mean annual basis with r-value = 0.33 and 0.39 and p-value = 0.14 and 0.08 respectively (Figure 5B and C).

The ratio of the intermediate axis over the long axis negatively correlates with the distance from the Western Escarpment (r-value = -0.33), but a strong and positive correlation is found with the mean slope angles of the basins (r-value = 0.63; p-value = 0.01; Figure 5D).

4. DISCUSSION

4.1 CONTROLS ON GRAIN SIZE

Downstream fining trends in the Majes basin indicate fluvial controls

In fluvial environments, the sorting of the sediment depends on the downstream distance from its source (Hoey and Ferguson, 1994; Kodoma, 1994; Paola and Seal, 1995). This is particularly the case for the Majes river, where the sorting gets better in the downstream direction. In particular, we do see an exponential downstream fining trend of the three percentiles in the Majes river (Figure 4). This is somewhat surprising because sufficiently voluminous sediment input from other sources may perturb any downstream fining trends in the grain size distribution (Rice and Church, 1998). Likewise, in the Majes basin, the sediment supply from the hillslopes to the trunk stream has occurred mainly through debris flow processes and landsliding (Steffen et al., 2010; Margirier et al., 2015). Accordingly, while the supply of hillslope-dervied material is likely to have been accomplished by mass wasting processes, the evacuation and transport of this sediment down to the Pacific Ocean has predominantly occurred through fluvial transport, as the exponential downstream fining of the grains implies.

Absence of gravels in rivers between 15.6°S and 13.7 °S

In the rivers located between 15.6°S and 13.7°S, no gravel bars are encountered where these rives leave the mountain range, and only sand bars can be found. This suggests that the transition from a gravel- to a sand-covered bed, i.e. the gravel front, is located along a more upstream reach of these rivers. This transition is generally rapid (Dingle et al., 2017) and often associated with a break in slope (Knighton, 1999). The gravel-sand transition has been interpreted to be controlled by either the elevation of the local base level, an excess of sand supply, and breakdown of fine gravels by abrasion (Dingle et al., 2017), or a combination of these parameters (Knighton, 1999). In our case, these rivers do not show any particular differences compared to the other rivers where coastal gravel bars have been found. In particular, there is no particular evidence why preferential breakdown of gravels along these rivers should be more efficient than in rivers farther north and south because the upstream morphometry and bedrock geology is similar. The other explanation would be an excess of sand supplied to these rivers. However, available information and geological maps do not display any major differences in bedrock lithologies along strike (Figure 1B), but we note that the resolution of the geological map does not provide enough detail about the weathering of the bedrock or the amount of regolith, which could be a source of sand. However, these rivers are situated in the segment where the buoyant Nazca Ridge is being subducted beneath the South American continental plate (Figure 3), which resulted in an uplift pulse of the forearc during Pliocene-Quaternary times, accompanied by enhanced erosion on the surface and at interface between the subducting and the hangingwall plate through tectonic shear (Hampel, 2002; Hampel et al., 2004). These effects are generally recorded in the morphology and sedimentary facies of the forearc (Hampel, 2002). Additionally, based on a detailed morphometric analysis of the region, Wipf et al. (2008) showed that this coastal uplift has rerouted and deflected the rivers in this area and has lengthened the downstream end of these rivers. It is thus possible that these tectonically-driven mechanisms caused the gravel front to step back farther into the mountain range, with the effect that the downstream terminations of these rivers only display sand bars. But we note that this interpretation warrants further detailed investigations, which includes a down-stream survey of the sediments in these rivers from the headwaters to the site where they discharge into the Pacific Ocean (similar to the analyses made along the Majes river, please see above).

Grain size and earthquake frequency

Landslides and debris flows represent the main processes of hillslope erosion and the main source of sediment in tectonically active orogens (Hovius et al., 1997; Korup et al., 2011). They are generally associated with triggers such as earthquakes and generally supply coarse and voluminous sediments to the trunk rivers (Dadson et al., 2003; McPhillips et al., 2014). In that sense we would infer a positive correlation between the frequency of large earthquakes and the grain size where an increase of earthquake frequency would induce an increase of landslide occurrence, thereby supplying coarser grained sediment from the hillslopes to the rivers. However, no correlation has been found between the seismicity and the grain size data when looking at the number of recorded historical earthquakes (Figure 3). We then infer that seismic activity and particularly the subduction mechanisms do not exert a measurable control on the grain size in the rivers of the western Peruvian Andes. Nevertheless, we do consider that the lack of gravels in rivers where the subduction of the buoyant Nazca ridge has caused uplift of the hangingwall plate was explained by a tectonic driving force (see section above). In particular, since this uplift caused a re-routing of these rivers (Wipf et al., 2006) and thus a lengthening of the river courses, the gravel front might have stepped back relative to the river mouth into the Pacific Ocean, as we have noted above.

Supply control on the grain size pattern

Because we have found positive correlations between the D_{50} and the basins scale properties (basin area, mean basin slope, mean basin denudation rates, water shear stresses, sediment fluxes), we infer that the mean grain size reflects the ensemble of a complex pattern of erosional and sediment transport processes operating in the Peruvian basins. In particular, the positive correlation between the size of the D_{50}, the basin averaged denudation rate and the morphometry of these basins leads us to propose that environmental factors exert a major control on the pattern of the D_{50} encountered for the rivers in western Peru. In this context, it is very likely that the bulk supply of hillslope-derived sediment to the trunk stream increases with larger basin size, mean basin slope and basin-averaged denudation rate, as the recent study by Reber et al. (in press) has revealed. Furthermore, while tectonic processes such as earthquake frequencies have no measurable impact on the grain size pattern, as we have outlined above, we consider it more likely that hillslope processes occurred in response to strong precipitation events, as suggested Bekaddour et al. (2014) and as recently shown by the devastating mudflows and floods in coastal Peru (March 2017) due to an El Niño event. The consequence is that higher denudation rates, and larger basins, result in a larger sediment flux in the trunk stream, which in turn yields an increase in the scale at which transport and deposition of material occurs (Armitage et al., 2011). Related mechanisms are likely to shift gravel fronts in rivers towards more distal sites, which could positively influence the mean grain size percentile of the trunk rivers in the sense that the material will coarsen.

We note that following the results from the Majes basin, we would expect a decrease in the size of the D_{50} for larger basins and larger distances from the uppermost edge of the Western Escarpment, because of larger transport distances and thus a higher impact related to any downstream fining trends. While these mechanisms, i.e, fining trends of all percentiles, are likely to be observed at the scale of individual basins, we do not consider that transport distance alone is capable of explaining the D_{50} pattern in rivers at the scale of the entire western Andean margin of Peru. In particular, the fining rate not only depends on the abrasion (Dingle et al., 2017) and the selective entrainment processes upon transport (Ashword and Ferguson, 1989), but also on the rate at which sediment is supplied to the rivers (e.g. McLaren, 1981; McLaren and Bowles, 1985). Particularly, in basins where the rate of hillslope-derived supply of sediment from the hillslopes to the trunk stream is large, the overall downstream fining rate of the material is expected to be less, because lateral sediment pulses are likely to cause the grain size fraction to increase. This has been exemplified for modern examples in the Swiss Alps (Bekaddour et al., 2013) and for the Pisco river in Peru (Litty et al., 2016), where fining rates of modern stream sediment, which record low denudation rates (Bekaddour et al., 2014), are greater than those of Pleistocene fluvial terraces, which record fast paleo-denudation rates (Bekaddour et al., 2014). Support for this interpretation is also provided by the positive correlation between the D_{50} and the mean basin denudation rate, where larger hillslope-derived material is likely to increase the overall sediment flux within the rivers. The consequence is a downstream shift of the gravel front and thus of the larger size fraction of the material, as we have interpreted above.

Hydrological control on the grain size distribution

Hydrodynamic conditions of rivers influence the grain size upon entrainment, transport, and deposition (Hjulström, 1935; Komar and Miller 1973; Surian, 2002). In this sense, rivers with larger shear stresses are capable of transporting larger clasts. Accordingly, at equilibrium conditions, we expect a correlation between the grain-size distributions and the shear stresses exerted by the water at our surveying sites, because greater flow strengths are required to entrain the coarser fractions of the material that make up the river beds (e.g., Ferguson et al. 1989; Komar and Shih 1992). This is the case in our study where the grain sizes correlate with the shear stress values. Interestingly, the correlation coefficients between the shear stress and the grain size percentiles increase from 0.23 for the D_{50} to 0.33 for the D_{84} and to 0.39 for the D_{96}. This suggests that the shear stress exerted by mean annual water flows has a greater impact on the coarse fractions than on the fine fractions of the stream sediments. While we cannot fully explain why the larger percentiles reveal a better correlation with shear stresses of mean annual flow conditions with the available dataset, we do infer a hydraulic control on grain size distribution of the Peruvian rivers.

4.2 TRANSPORT DISTANCE AND SLOPE ANGLE CONTROLS ON SPHERICITY

We consider a control of the transport distance on the sphericity of the pebbles. We indeed see a negative correlation between the sphericity and the distance from the Western Escarpment where the major sediment sources are situated, as provenance tracing investigations have shown (Litty et al., 2017). This suggests a decrease of the sphericity with a larger transport distance. As particles are transported over longer distances, we actually would expect abrasion (Dingle et al.,

2017) to equalize the length of the three axes, thus making a particle more spherical. While this concept is likely to be valid for pebbles with a homogenous fabric, it likely fails to describe the abrasion and break-down of material with an inherited planar geologic fabric (such as gneisses and sediments). Indeed, pebbles flatten as effects of abrasion and 3D heterogeneities of bedrock that becomes more obvious with time and transport distance (Sneed and Folk, 1958). We note that this is only valid if we assume a linear correlation between river length and transport time. The reincorporation of previously abraded gravels from earlier erosion and multiple transport cycles of clasts that were temporarily stored in cut-and-fill terrace sequences, as e.g., put forward by Bekaddour et al. (2014) in their study about cut-and-fill terraces in the Pisco valley at c. 13.7°S latitude, would positively contribute to this effect upon increasing the time scale of sediment evacuation.

Additionally, we consider a control of the mean catchment slope on the sphericity of the pebbles, where correlations are positive, i.e. the steeper a basin the rounder the pebbles (Figure 5). We do not consider that this pattern is due to differences in exposed bedrock in the hinterland because the litho-tectonic architecture is fairly constant along the entire Peruvian margin (Figure 1). Instead, the observations point toward the same control mechanisms on the pebble sphericity as noted above. Steeper slope angles are most likely associated with faster denudation rates as the Peruvian study by Reber et al. (in press) has shown. Accordingly, we infer a shorter transport distance of the material and thus a shorter time scale of transport compared to the evacuation time in long and less steep rivers. Similar to what we have noted above, we see the positive correlation between mean hillslope angle and the sphericity of pebbles as a very likely consequence of shorter transport times in steeper basins, but we note that this hypothesis needs to be confirmed by detailed real-time surveys of material transport from sources down to the end of these rivers.

Conclusion

We have conducted a grain size analysis of gravel bars in all major rivers that are situated on the western Andean margin of Peru where they leave the mountain belt. We have not found any correlations to the current seismic regimes, where a larger seismicity is expected to increase the supply of coarse-grained material. Instead, we found positive correlations between water shears stresses, mean basin denudation rates, mean basin slopes and basin sizes on nearly all grain size percentiles. We interpret these results as the combined effect of various geomorphic conditions where larger denudation rates operating in larger basins, and steeper slopes, paired with larger flow shear stresses, are capable of transporting more and coarser-grained material. Furthermore, we unravel a transport time control on the shape of the clasts where steeper slopes and smaller basins (i.e., shorter distances to the edge of the Western Escarpment) are anticipated to shorten the residence time of the clasts in the system, thereby yielding more spherical clasts. In particular, longer residence times would allow abrasion to be more selective because of a planar lithologic fabric of most of the clasts, which in turn, would cause clasts to flatten upon longer exposure towards abrasion. This suggest that the ensemble of erosional and sediment transport processes have reached an equilibrium at the scale of individual clasts, but also at the reach scale of rivers where the sedimentary architecture and the clast fabric of the channel fill has dynamically adjusted to water and sediment flux and their specific time scales. Accordingly, we see the western Peruvian margin as ideal laboratory to analyze the relationships between sediment supply and water runoff on the grain size pattern of the bedload, and we propose that the bedload caliber of these streams has reached an equilibrium to environmental conditions including water discharge, sediment flux and channel geometries.

ACKNOWLEDGMENTS

This project is funded by the Swiss National Science Foundation (project Number 137516).

REFERENCES CITED

Abbühl, L.M., Norton, K.P., Jansen, J.D., Schlunegger, F., Aldahan, A., and Possnert, G., 2011, Erosion rates and mechanisms of knickzone retreat inferred from 10Be measured across strong climate gradients on the northern and central Andes Western Escarpment: Earth Surface Processes and Landforms, v. 36, p. 1464–1473.

Allen, G. H., Barnes, J. B., Pavelsky, T. M. and Kirby, E., 2013, Lithologic and tectonic controls on bedrock channel form at the northwest Himalayan front: Journal of Geophysical Research: Earth Surface, v. 118, no. 3, p. 1806-1825.

Allen, P. A., Michael, N. A., D'Arcy, M., Roda-Boluda, D. C., Whittaker, A. C., Duller, R. A., and Armitage, J. J., 2016. Fractionation of grain size in terrestrial sediment routing systems. Basin Research.

Armitage, J. J., Duller, R. A., Whittaker, A. C., and Allen, P. A., 2011. Transformation of tectonic and climatic signals from source to sedimentary archive. Nature Geoscience, 4(4), 231-235.

Ashworth, P. J. and Ferguson, R. I., 1989. Size-selective entrainment of bed load in gravel bed streams. Water Resources Research, v. 25(4), p. 627-634.

Atherton, M. P., 1984. The coastal batholith of Peru. In Andean Magmatism (pp. 168-179). Birkhäuser Boston.

Attal, M. and Lavé, J., 2006, Changes of bedload characteristics along the Marsyandi River (central Nepal): Implications for understanding hillslope sediment supply, sediment load evolution along fluvial networks, and denudation in active orogenic belts: Geological Society of America Special Papers, v. 398, p.143-171.

Attal, M. and Lavé, J., 2009. Pebble abrasion during fluvial transport: experimental results and implications for the evolution of the sediment load along rivers. J. Geophys. Res. 114:F04023. doi:10.1029/2009JF001328.

Attal, M., Mudd, S. M., Hurst, M. D., Weinman, B., Yoo, K. and Naylor, M., 2015, Impact of change in erosion rate and landscape steepness on hillslope and fluvial sediments grain size in the Feather River basin (Sierra Nevada, California): Earth Surface Dynamics, v. 3, p. 201-222.

Bekaddour, T., Schlunegger, F., Attal, M., and Norton, K. P, 2013. Lateral sediment sources and knickzones as controls on spatio-temporal variations of sediment transport in an Alpine river. Sedimentology, v. 60(1), p. 342-357.

Bekaddour, T., Schlunegger, F., Vogel, H., Delunel, R., Norton, K. P., Akçar, N., and Kubik, P., 2014. Paleo erosion rates and climate shifts recorded by Quaternary cut-and-fill sequences in the Pisco valley, central Peru. Earth and planetary science letters, v. 390, p. 103-115.

Blissenbach, E., 1952. Relation of surface angle distribution to particle size distribution on alluvial fans: J. Sediment. Petrol., v. 22, p. 25–28.

Bookhagen, B. and Strecker, M. R., 2008, Orographic barriers, high-resolution TRMM rainfall, and relief variations along the eastern Andes, Geophysical Research Letters, v. 35, p. L06403.

Bunte, K., Abt, S.R., 2001a. Sampling frame for improving pebble count accuracy in coarse gravel-bed rivers. Journal of the American Water Resources Association, v. 37 (4), p. 1001- 1014.

Bunte, K., Abt, S.R., 2001b. Sampling surface and subsurface particle-size distributions in wadable gravel- and cobble-bed rivers for analyses in sediment transport, hydraulics, and streambed monitoring. General Technical Report RMRS-GTR-74. United States Department of Agriculture; Forest Service; Rocky Mountain Research Station. Fort Collings, USA, p. 428.

Carretier, S., Tolorza, V., Rodríguez, M. P., Pepin, E., Aguilar, G., Regard, V. and Hérail, G., 2015. Erosion in the Chilean Andes between 27° S and 39° S: tectonic, climatic and geomorphic control. Geological Society, London, Special Publications, v. 399(1), p. 401-418.

Dadson, S. J., Hovius, N., Chen, H., Dade, W. B., Hsieh, M. L., Willett, S. D. and Lague, D., 2003. Links between erosion, runoff variability and seismicity in the Taiwan orogen. Nature, v. 426(6967), p. 648-651.

DeVries, T. J., 1987, A review of geological evidence for ancient El Nino activity in Peru. J. Geophys. Res, v. 92, no. 14, p. 471–14.

Dingle, E. H., Attal, M., and Sinclair, H. D., 2017. Abrasion-set limits on Himalayan gravel flux. Nature, v. 544(7651), p. 471-474.

Duller, R. A., Whittaker, A. C., Swinehart, J. B., Armitage, J. J., Sinclair, H. D., Bair, A. and Allen, P. A., 2012, Abrupt landscape change post-6 Ma on the central Great Plains, USA: Geology, v. 40, p. 871-874.

Fedele, J. J. and Paola C., 2007, Similarity solutions for fluvial sediment fining by selective deposition: Journal of Geophysical Research: Earth Surface (2003–2012), v. 112.

Ferguson, R. I., Prestegaard, K. L. and Ashworth, P. J., 1989. Influence of sand on hydraulics and gravel transport in a braided gravel bed river. Water Resources Research, v. 25(4), p. 635-643.

Foreman, B. Z., Heller, P. L. and Clementz, M. T., 2012, Fluvial response to abrupt global warming at the Palaeocene/Eocene boundary: Nature, v. 491, no. 7422, p. 92-95

Foreman, B. Z., 2014, Climate-driven generation of a fluvial sheet sand body at the Paleocene–Eocene boundary in north-west Wyoming (USA): Basin Research, v. 26, no. 2, p. 225-241.

Garreaud, R. D., Vuille, M., Compagnucci, R., and Marengo, J., 2009, Present-day South American climate. Palaeogeography, Palaeoclimatology, Palaeoecology, v. 281, no. 3, p. 180-195.

Haederle, M. and Atherton, M. P., 2002. Shape and intrusion style of the Coastal Batholith, Peru. Tectonophysics, v. 345(1), p. 17-28.

Hampel, A., 2002. The migration history of the Nazca Ridge along the Peruvian active margin: a re-evaluation. Earth and Planetary Science Letters, v. 203(2), p.665-679.

Hampel, A., Adam, J., and Kukowski, N., 2004. Response of the tectonically erosive south Peruvian forearc to subduction of the Nazca Ridge: Analysis of three-dimensional analogue experiments. Tectonics, 23(5).

Hancock, G. S. and Anderson, R. S., 2002. Numerical modeling of fluvial strath-terrace formation in response to oscillating climate. Geological Society of America Bulletin, v. 114(9), p. 1131-1142.

Heller, P. L. and Paola, C., 1992, The large-scale dynamics of grain-size variation in alluvial basins, 2: Application to syntectonic conglomerate: Basin Research, v. 4, no. 2, p. 91-102.

Hjulström, F., 1935, Studies in the morphological activity of rivers as illustrated by the river Fyris: Bulletin of the Geological Institution of the University of Uppsala, v 25, p. 221-528.

Hoey, T. B. and Ferguson, R., 1994, Numerical simulation of downstream fining by selective transport in gravel bed rivers: Model development and illustration: Water resources research, v.30, p. 2251-2260.

Hovius, N., Stark, C. P. and Allen, P. A., 1997. Sediment flux from a mountain belt derived by landslide mapping. Geology, v. 25(3), p. 231-234.

Howard, J.L., 1993. The statistics of counting clasts in rudites: a review with examples from the upper Paleogene of southern California, USA. Sedimentology 40, 157-174.

Huffman, G. J., Bolvin, D. T., Nelkin, E. J., Wolff, D. B., Adler, R. F., Gu, G. and Stocker, E. F., 2007, The TRMM multisatellite precipitation analysis (TMPA): Quasi-global, multiyear, combined-sensor precipitation estimates at fine scales. Journal of Hydrometeorology, v. 8, no. 1, p. 38-55.

Isacks, B. L., 1988. Uplift of the central Andean plateau and bending of the Bolivian orocline. Journal of Geophysical Research: Solid Earth, v. 93(B4), p. 3211-3231.

Knighton, A. D., 1999. The gravel–sand transition in a disturbed catchment. Geomorphology, v. 27(3), p. 325-341.

Kodoma, Y., 1994, Downstream changes in the lithology and grain size of fluvial gravels, the Watarase River, Japan: Evidence of the role of abrasion in downstream fining: Journal of Sedimentary Research, Section A: Sedimentary Petrology and Processes, v. 64A, p. 68-75.

Koiter, A. J., Owens, P. N., Petticrew, E. L. and Lobb, D. A., 2013, The behaviour characteristics of sediment properties and their implications for sediment fingerprinting as an approach for identifying sediment source sin river basins: Earth Science Reviews, v. 125, p. 24-42.

Komar, P. D. and Miller, M. C., 1973. The threshold of sediment movement under oscillatory water waves. Journal of Sedimentary Research, v. 43(4).

Komar, P. D. and Shih, S. M., 1992. Equal mobility versus changing bedload grain sizes in gravel-bed streams. Dynamics of gravel-bed rivers, p. 73-106.

Korup, O. and Schlunegger, F., 2009. Rock-type control on erosion-induced uplift, eastern Swiss Alps. Earth and Planetary Science Letters, v. 278(3), p. 278-285.

Korup, O. and Weidinger, J. T., 2011. Rock type, precipitation, and the steepness of Himalayan threshold hillslopes. Geological Society, London, Special Publications, v. 353(1), p. 235-249.

Lisle, T.E., Iseya, F. and Ikeda, H., 1993, Response of a channel with alternate bars to a decrease in supply of mixed-size bed load: A flume experiment: Water resources research, v. 29, p. 3623–3629.

Litty, C., Duller, R., and Schlunegger, F., 2016. Paleohydraulic reconstruction of a 40 ka-old terrace sequence implies that water discharge was larger than today. Earth surface processes and landforms.

Litty and Schlunegger, 2017. Controls on Pebbles' Size and Shape in Rivers of the Swiss Alps. The Journal of Geology., v. 125, p. 101–112.

Litty, C., Lanari, P., Burn, M., and Schlunegger, F., 2017, Climate-controlled shifts in sediment provenance inferred from detrital zircon ages, Western Peruvian Andes. Geology. v. 45; no. 1; p. 59–62.

Marcus, W.A., Ladd, S.C., Stoughton, J.A., Stock, J.W., 1995. Pebble counts and the role of user-dependent bias in documenting sediment size distributions. Water Resources Research, v. 31 (10), p. 2625-2631.

Margirier, A., Audin, L., Carcaillet, J., Schwartz, S., and Benavente, C., 2015, Tectonic and climatic controls on the Chuquibamba landslide (western Andes, southern Peru). Earth Surface Dynamics, 3(2), 281-289.

McLaren, P., 1981. An interpretation of trends in grain size measures. Journal of Sedimentary Research, 51(2).

McLaren, P. and Bowles, D., 1985, The Effects of Sediment Transport on Grain-Size Distributions: Journal of Sedimentary Petrology, v. 55, p. 457-470.

McPhillips, D., Bierman, P. R., & Rood, D. H., 2014. Millennial-scale record of landslides in the Andes consistent with earthquake trigger. Nature Geoscience, v. 7(12), p. 925-930.

Montgomery, D. R., Balco, G. and Willett, S. D., 2001. Climate, tectonics, and the morphology of the Andes. Geology, v. 29(7), p. 579-582.

Mukasa, S. B., 1986. Zircon U-Pb ages of super-units in the Coastal batholith, Peru: Implications for magmatic and tectonic processes. Geological Society of America Bulletin, v. 97(2), p. 241-254.

Nocquet, J. M., Villegas-Lanza, J. C., Chlieh, M., Mothes, P. A., Rolandone, F., Jarrin, P. and Martin, X., 2014. Motion of continental slivers and creeping subduction in the northern Andes. Nature Geoscience, v. 7(4), p. 287-291.

Ouimet, W. B., Whipple, K. X., & Granger, D. E., 2009. Beyond threshold hillslopes: Channel adjustment to base-level fall in tectonically active mountain ranges. Geology, v. 37(7), p. 579-582.

Paola, C., Heller, P. L. and Angevinet, C. L., 1992a, The large-scale dynamics of grain-size variation in alluvial basins, 1: Theory: Basin Research, v. 4, p. 73-90.

Paola, C. and Seal, R., 1995, Grain size patchiness as a cause of selective deposition and downstream fining: Water Resources Research, v. 31, p. 1395-1407.

Parker, G., 1991, Selective sorting and abrasion of river gravel. 1: Theory: Journal of Hydraulic Engineering, v. 117, no. 2, p. 131-147.

Pearson, K., 1895, Notes on regression and inheritance in the case of two parents, Proceedings of the Royal Society of London, v. 58, p. 240–242.

Ramos, V. A., 2010. The tectonic regime along the Andes: Present-day and Mesozoic regimes. Geological Journal, v. 45(1), p. 2-25.

Rasband, W.S., ImageJ, U. S. National Institutes of Health, Bethesda, Maryland, USA, http://imagej.nih.gov/ij/, 1997-2016.

Reber, R., Delunel, R., Schlunegger, F., Litty, C., Madella, A., Akçar, N., Christl, M. In press in Terra Nova. Environmental controls on 10Be-based catchment averaged denudation rates along the western margin of the Peruvian Andes.

Regard, V., Saillard, M., Martinod, J., Audin, L., Carretier, S., Pedoja, K. and Hérail, G., 2010. Renewed uplift of the Central Andes Forearc revealed by coastal evolution during the Quaternary. Earth and Planetary Science Letters, v. 297(1), p. 199-210.

Reuter, H. I., Nelson, A. and Jarvis, A., 2007. An evaluation of void-filling interpolation methods for SRTM data. International Journal of Geographical Information Science, v. 21(9), p. 983-1008.

Rice, S. and Church, M., 1998, Grain size along two gravel-bed rivers: Statistical variation, spatial pattern and sedimentary links: Earth Surface Processes and Landforms, v. 23, p. 345-363.

Robinson, R. A. and Slingerland, R. L., 1998, Origin of fluvial grain-size trends in a foreland basin: the Pocono Formation on the central Appalachian basin: Journal of Sedimentary Research, v. 68, no. 3.

Schildgen, T. F., Hodges, K. V., Whipple, K. X., Reiners, P. W. and Pringle, M. S., 2007, Uplift of the western margin of the Andean plateau revealed from canyon incision history, southern Peru. Geology 35, 523–526.

Schumm, S. A. and Stevens, M. A., 1973, Abrasion in place: a mechanism for rounding and size reduction of coarse sediments in rivers: Geology, v. 1, p. 37-40.

Shields, A., 1936, Anwendung der Ahnlichkeitsmekanik und der Turbulenzforschung auf die Geschiebebewegung, Mittelung der preussischen Versuchsanstalt für Wasserbau und Schiffbau, 26. (Berlin).

Sneed, E.D., and Folk, R.L., 1958. Pebbles in the lower Colorado River, Texas a study in particle morphogenesis. The Journal of Geology, 114-150.

Steffen, D., Schlunegger, F., and Preusser, F., 2010, Late Pleistocene fans and terraces in the Majes valley, southern Peru, and their relation to climatic variations. International Journal of Earth Sciences, v. 99(8), p. 1975-1989.

Sternberg, H., 1875, Untersuchungen über längen-und Querprofil geschiebeführender Flüsse, Z. Bauwes., 25, 486–506.

Surian, N., 2002, Downstream variation in grain size along an Alpine river: analysis of controls and processes: Geomorphology, v. 43, p. 137-149.

Trauerstein, M., Norton, K. P., Preusser, F., and Schlunegger, F., 2013, Climatic imprint on landscape morphology in the western escarpment of the Andes. Geomorphology, v. 194, p. 76-83.

Van den Berg, F., and Schlunegger, F., 2012. Alluvial cover dynamics in response to floods of various magnitudes: The effect of the release of glaciogenic material in a Swiss Alpine catchment. Geomorphology, v. 141, p. 121-133.

Vidal, J. C., 1993, Geologia de los cuadrangulos de Huambo y Orcopampa, v 46. Instituto Geologico Minero y Metalurgico, Lima.

Whittaker, A. C., Cowie, P. A., Attal, M., Tucker, G. E. and Roberts, G. P., 2007, Bedrock channel adjustment to tectonic forcing: Implications for predicting river incision rates: Geology, v. 35, no. 2, p.103-106.

Whittaker, A. C., Attal, M. and Allen, P.A., 2010, Characterising the origin, nature and fate of sediment exported from catchment perturbed by active tectonics. Basin Research. v. 22. p. 809-828.

Wittmann, H., von Blanckenburg, F., Kruesmann, T., Norton, K. P., and Kubik, P. W., 2007. Relation between rock uplift and denudation from cosmogenic nuclides in river sediment in the Central Alps of Switzerland. Journal of Geophysical Research: Earth Surface, 112(F4).

Wipf, M., Zeilinger, G., Seward, D., and Schlunegger, F., 2008. Focused subaerial erosion during ridge subduction: impact on the geomorphology in south-central Peru. Terra Nova, v. 20(1), p. 1-10.

FIGURES AND TABLES CAPTIONS

Table 1: Location of the sampling sites with the altitude in meters above sea level. The table also displays grain size results together with the rivers' and basins' properties and hydrological properties.

Table 2: Location of the sampling sites in the Majes basin and grain size results in the Majes basin.

Table 3: Results of the statistical investigations, illustrated here as correlation matrix of the r-values. The valuess in bold show significant correlation between the grain size data and the different catchment scale properties.

Table 4: Results of the statistical investigations, illustrated here as correlation matrix of the p-values. The values in bold have a significance level alpha < 0.1

Figure 1: A: Map of the studied basins showing the sampling sites and the western escarpment (western escarpment modified after Trauerstein et al., 2013). The southern and northern group of basins represent catchments displaying differences in terms of their sizes and relationships with grain sizes (see Results) **B:** Geological map of the western Peruvian Andes. **C:** Map of the precipitation rates showing the spatial extend of the ITCZ, modified after Huffman et al., 2007.

Figure 2: Geological map of the Majes basin overlain by the precipitation pattern (Precipitation data from Steffen et al., 2010., where the black dashed lines show precipitation rates (mm/yr). GS1 to GS5 represent sites where grain size data has been collected. The right corner shows the Majes river long profile.

Figure 3: Topography of subducting Nazca plate, where slab depth data has been extracted from earthquake.usgs.gov/data/slab/. This N-S projection also illustrates: a) tectonic lineaments such as submarine ridges and MFZ: Mendaña Fracture Zone; NFZ: Nazca Fracture Zone; b) Holocene Volcanoes; c) Earthquake data, taken from earthquake.usgs.gov/earthquakes/search/; number of earthquakes M>4 within 30 km radius window. d) Coastal elevation. The data has been extracted

from a 20 km-wide swath prole along the coast. The three lines represent maximum, mean and minimum elevations within the selected swath; e) Catchment averaged denudation rates have been corrected for quartz contents (Reber et al. in press); f) Mean annual precipitation rates (Reber et al., in press); g) Mean annual water discharge (Reber et al., in press); h) Grain size results for the intermediate (b)-axis of the pebbles in the rivers from north to south at the sampling sites presented in Figure 1; i) Ratio between the intermediate axis and the long (a)-axis (modied after Reber et al., in press).

Figure 4: Grain size results along the Majes River.

Figure 5: Correlations between the grain size data and the river parameters. **A:** D_{50} versus sediment fluxes. **B:** D_{84} versus shear stress exerted by the water. **C:** D_{96} versus shear stress exerted by the water. **D:** Ratio b/a versus mean catchment slope.

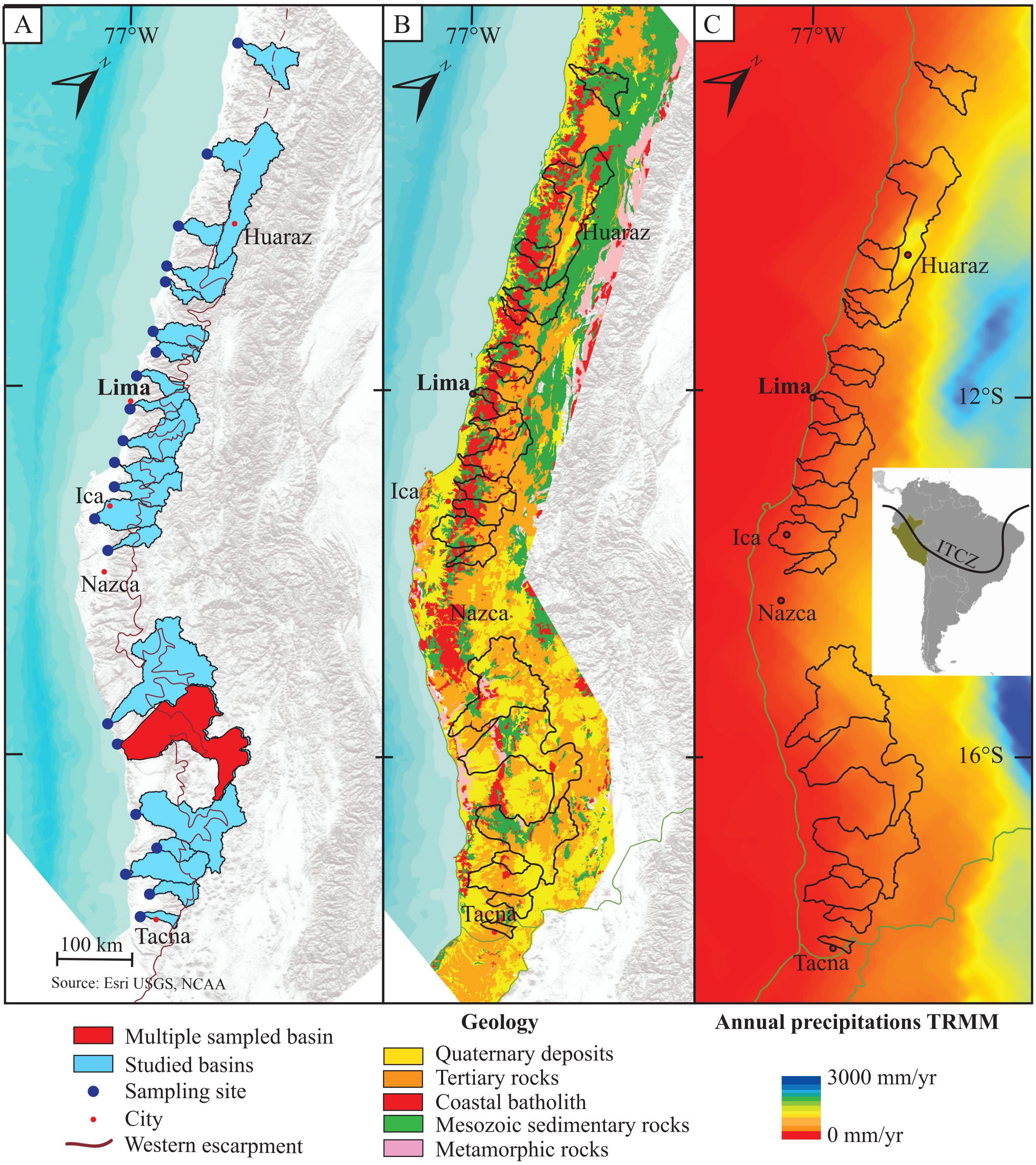

Figure 1: A: Map of the studied basins showing the sampling sites and the western escarpment (western escarpment modified after Trauerstein et al., 2013). **B:** Geological map of the western Peruvian Andes. **C:** Map of the precipitation rates showing the spatial extend of the ITCZ, modified after Huffman et al., 2007.)

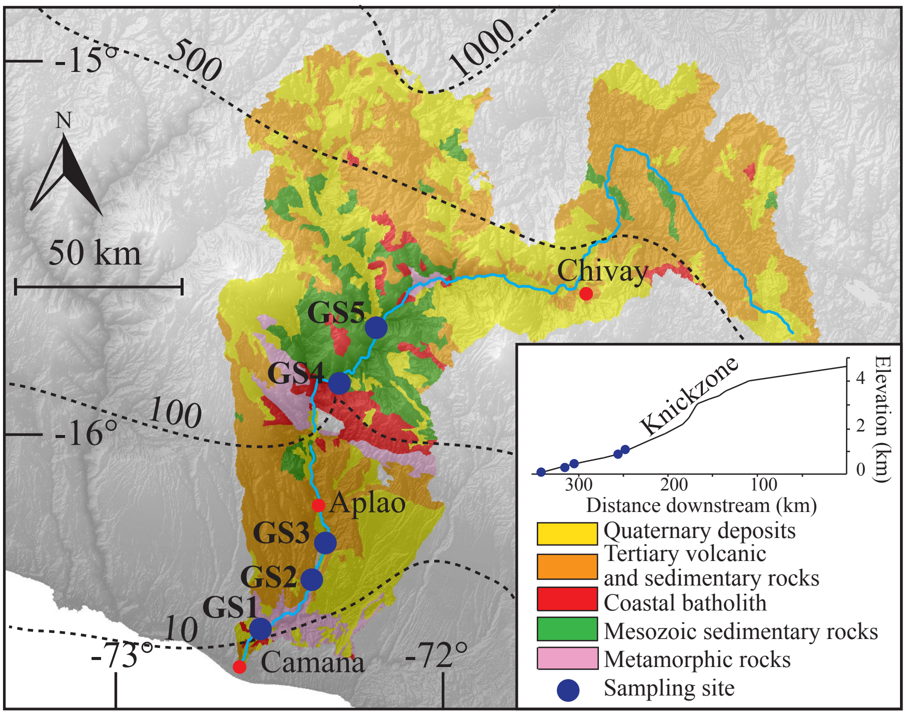

Figure 2: Geological map of the Majes basin overlain by the precipitation pattern (Precipitation data from Steffen et al., 2010., where the black dashed lines show precipitation rates (mm/yr). GS1 to GS5 represent sites where grain size data has been collected. The right corner shows the Majes river long profile.

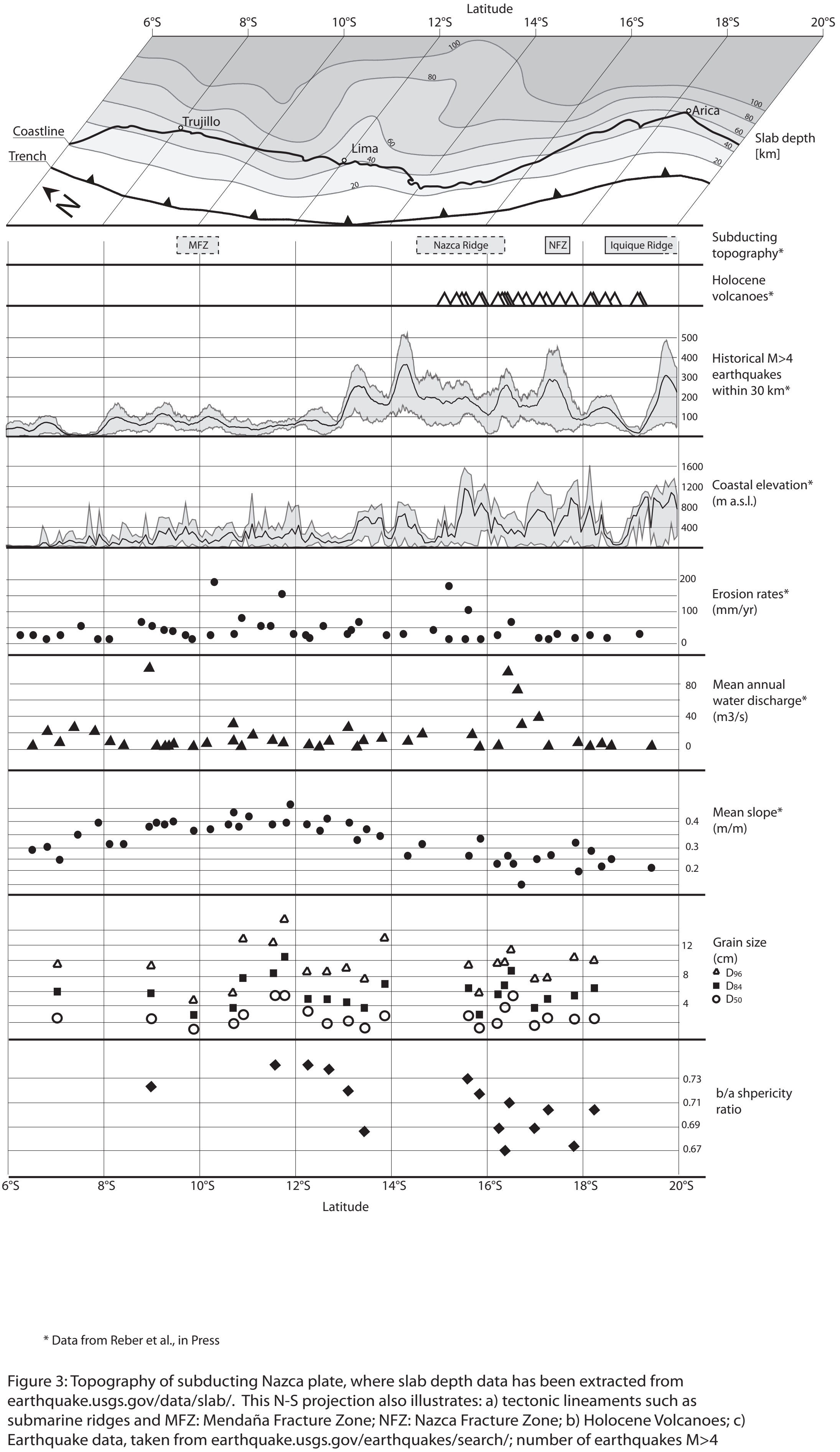

* Data from Reber et al., in Press

Figure 3: Topography of subducting Nazca plate, where slab depth data has been extracted from earthquake.usgs.gov/data/slab/. This N-S projection also illustrates: a) tectonic lineaments such as submarine ridges and MFZ: Mendaña Fracture Zone; NFZ: Nazca Fracture Zone; b) Holocene Volcanoes; c) Earthquake data, taken from earthquake.usgs.gov/earthquakes/search/; number of earthquakes M>4 within 30 km radius window; d) Coastal elevation. The data has been extracted from a 20 km-wide swath profile along the coast. The three lines represent maximum, mean and minimum elevations within the selected swath; e) Catchment averaged denudation rates have been corrected for quartz contents; f) Mean annual water discharge; g) Mean basin slope. h) Grain size results for the intermediate (b)-axis of the pebbles in the streams from north to south at the sampling sites presented in Figure 1; i) Ratio between theintermediate axis and the long (a)-axis (modified after Reber et al., in press).

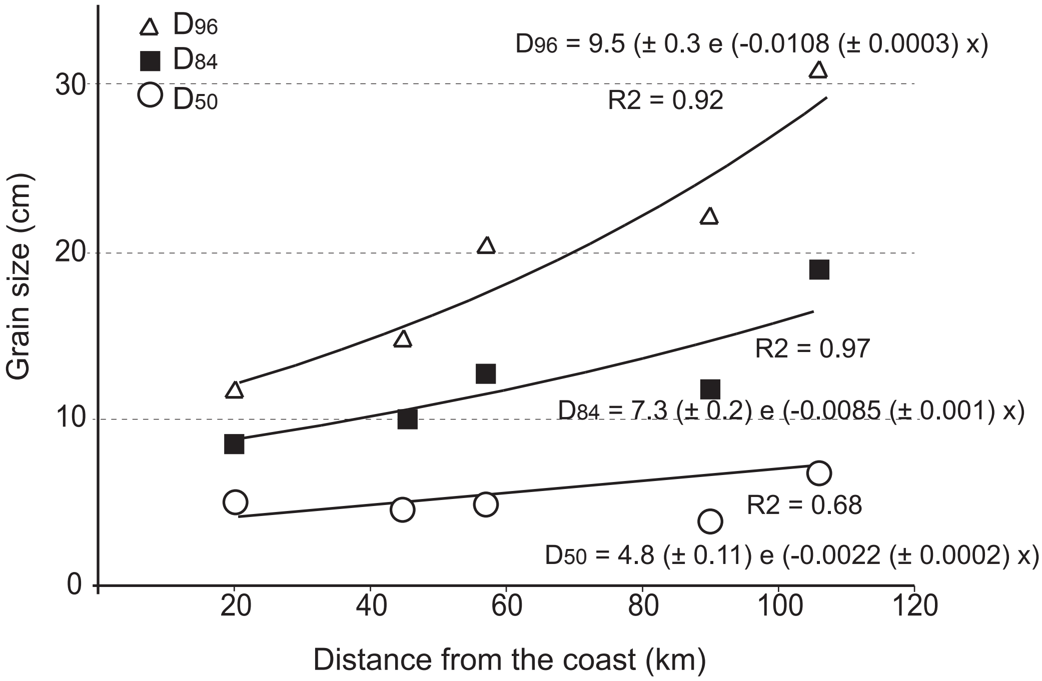

Figure 4: Grain size results along the Majes River.

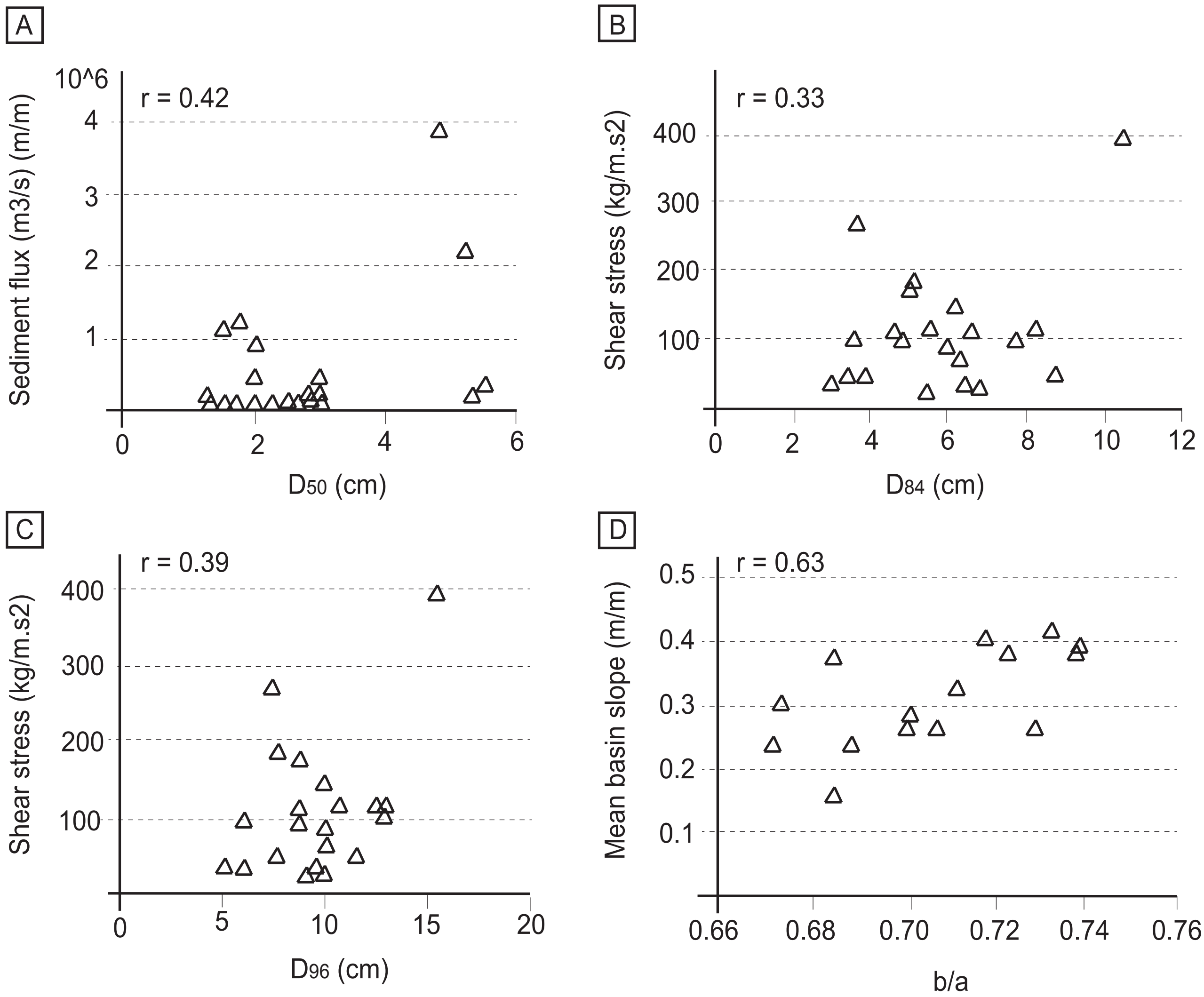

Figure 5: Correlations between the grain size data and the river parameters.
A: D50 versus sediment fluxes. B: D84 versus shear stress exerted by the water.
C: D96 versus shear stress exerted by the water. D: Ratio b/a versus mean catchment slope.

River name	Sample name	Altitude (m)	Latitude (DD WGS84)	Longitude (DD WGS84)	D50 (cm)	D84 (cm)	D96 (cm)	b/a	Catchment area (km2)	Mean slope (m/m) (Reber et al., in review)	Slope at the sampling site (m/m)	Distance form the western escarpment (km)	Channel width at the sampling site (m)	Mean annual water discharge (m3/s) (Reber et al., in review)	Shear stress (kg/m.s2)	Sediment flux (m3/s)	Denudation rates (mm/ka) (Reber et al., in review)	Denudation rates uncertainties (mm/ka) (Reber et al., in review)	Denudation rates corrected for Qz content in bedrock (mm/ka) (Reber et al., in review)
Tacna	PRC-ME1	231	-18.12	-70.33	2.3	6.2	10.0	0.70	899	0.28	0.015	48	6	3.4	142.68	11952	13.3	3.6	12.2
Rio Sama Grande	PRC-ME3	455	-17.82	-70.51	2.5	5.5	10.6	0.67	2150	0.3	0.013	73	6	4	114.14	61495	28.6	5.3	27.7
Ilo / Rio Osmore	PRC-ME5	1072	-17.29	-70.99	2.6	5.1	7.8	0.70	1783	0.26	0.018	53	7	3.4	184.18	38146	21.4	4.8	18.6
Rio Tambo	PRC-ME6	145	-17.03	-71.69	1.5	3.6	7.5	0.69	12885	0.24	0.051	141	26	38.1	265.69	1155744	89.7	16.7	72.1
Tambillo / Rio Sihuas	PRC-ME802	117	-16.34	-72.13	2.0	6.0	10.0	0.69	1708	0.15	0.019	70	15	30.1	88.78	58087	34	6.4	27.7
Camana / Rio Majes	PRC-ME7	69	-16.51	-72.64	5.2	8.7	11.6	0.67	17401	0.23	0.005	188	100	68.4	46.06	2218568	127.5	23.4	106.8
Ocona / Rio Ocona	PRC-ME9	14	-16.42	-73.12	4.8	6.8	10.0	0.71	16084	0.26	0.004	192	70	91.1	26.25	3893878	242.1	45	184.1
Nasca / Rio Grande	PRC-ME1402	15	-15.85	-74.26	1.3	3.0	6.0	0.71	1412	0.32	0.014	48	3	20.4	34.10	65093	46.1	8.6	29.4
Chacaltana / Rio Ica	PRC-ME15	3	-15.63	-74.64	2.9	6.4	9.6	0.73	4677	0.26	0.003	88	23	12.1	33.01	126266	27	5.7	25.1
Humay District / Rio Pisco	PRC-ME16	400	-13.73	-75.89	3	6.6	13		3649	0.34	0.013	62	20	13.6	112.91	379865	104.1	20.4	69.1
Chinca Alta / Rio San Juan	PRC-ME17	75	-13.47	-76.14	1.3	3.8	7.6	0.69	3090	0.37	0.01	78	5	10.1	48.54	189112	61.2	11.7	44.1
Rio Canete	PRC-ME19	23	-13.12	-76.39	2	4.6	8.8	0.72	6029	0.4	0.01	100	60	26.4	112.24	402743	66.8	12.3	51.2
Rio Omas	PRC-ME20	33	-12.67	-76.65	1.6	4.8	8.8	0.73	2322	0.41	0.0076	78	22	8.2	95.14	62913	27.1	5.4	17.9
Rio Lurin	PRC-ME22	40	-12.25	-76.89	3	5	8.8	0.74	1572	0.38	0.022	70	5	3.7	176.26	60515	38.5	7.1	23.6
Lima / Rio Chillon	PRC-ME39	402	-11.79	-76.99	5.3	10.5	15.5		1755	0.39	0.018	51	40	4.9	392.89	144272	82.2	15.5	53.4
Rio Chancay	PRC-ME23	72	-11.61	-77.24	5.5	8.3	12.5	0.74	3059	0.39	0.01	66	20	8.9	111.55	298866	97.7	18.4	52.8
Rio Supe	PRC-ME25	74	-11.07	-77.59	2.8	7.7	13		4306	0.38	0.012	82	5	3.8	98.55	179550	41.7	7.7	25.6
Rio Pativilca	PAT-ME	10	-10.72	-77.77	1.8	3.6	6		4607	0.44	0.014	74	30	30.9	96.30	1198281	260.1	48.8	190.9
Huarmey	PRC-ME38	24	-10.07	-78.16	1.7	3.4	5.2		2072	0.37	0.004	78	15	9.8	38.34	40816	19.7	4.5	10.1
Rio Santa	PRC-ME27	80	-8.97	-78.62	2	5.4	9	0.72	12313	0.38	0.005	65	40	96.1	23.08	876699	71.2	13.4	70.4
San Martin de Porres	PRC-ME30	67	-7.32	-79.48	2.9	6.3	10		3882	0.34	0.007	126	40	25.4	65.72	118401	30.5	5.9	25.8

Table 1 : Location of the sampling sites with the altitude in meters above sea level.
The table also displays grain size results together with the rivers' and basins' properties and hydrological properties.
Morphometric dataset for the sampled drainage basins. All calculations are based on the 90 m resolution DEM (NASA)
The precipitation, water discharge data and the denudation rates are from Reber et al., in review

	Distance from the coast (km)	Altitude (m)	Latitude (°)	Longitude (°)	D50	D84	D96	b/a
GS1	20	69	-16.51	-72.64	5.2	8.7	11.6	0.67
GS2	45	283	-16.37	-72.49	4.8	10	15	0.69
GS3	57	378	-16.28	-72.45	5.4	12.7	21	0.65
GS4	90	700	-16.00	-72.48	3.3	12	22.5	0.67
GS5	106	882	-15.86	-72.45	6.2	19	31	0.71

Table 2: Location of the sampling sites in the Majes basin and grain size results in the Majes basin.

	Altitude (m)	*Latitude (DD WGS84)*	*Longitude (DD WGS84)*	***D50 (cm)***	***D84 (cm)***	***D96 (cm)***	***b/a***	*Catchment area (km2)*	*Mean slope (m/m)*	*Distance form the western escarpment (km)*	*Mean annual water discharge (m3/s)*	*Shear stress (kg/m.s2)*	*Sediment flux (m3/s)*	*Denudation rates (mm/ka)*	*Denudation rates corrected for Qz content in bedrock (mm/ka)*
Altitude (m)	1.00														
Latitude (DD WGS84)	-0.36	1.00													
Longitude (DD WGS84)	0.46	-0.97	1.00												
D50 (cm)	0.09	0.00	-0.01	1.00											
D84 (cm)	0.14	0.04	-0.03	**0.87**	1.00										
D96 (cm)	0.18	0.02	-0.02	**0.73**	**0.93**	1.00									
b/a	-0.30	0.66	-0.71	0.09	0.00	-0.02	1.00								
Catchment area (km2)	-0.25	-0.12	0.12	**0.31**	0.16	0.04	-0.25	1.00							
Mean slope (m/m)	-0.23	0.72	-0.78	-0.07	-0.10	-0.03	**0.63**	-0.28	1.00						
Distance form the western escarpment (km)	-0.32	-0.14	0.14	**0.35**	0.16	0.03	**-0.33**	0.84	-0.35	1.00					
Mean annual water discharge (m3/s) (Reber et al., in review)	-0.30	0.03	-0.01	0.18	0.05	-0.07	-0.13	0.87	-0.23	0.64	1.00				
Shear stress (kg/m.s2)	0.45	-0.11	0.14	**0.23**	**0.33**	**0.39**	-0.06	-0.21	0.06	-0.23	-0.37	1.00			
Sediment flux (m3/s9	-0.23	-0.19	0.17	**0.42**	0.17	0.03	-0.21	0.86	-0.24	0.82	0.80	-0.22	1.00		
Denudation rates (mm/ka) (Reber et al., in review)	-0.23	0.04	-0.09	**0.34**	0.09	0.00	-0.09	0.56	0.12	0.48	0.56	-0.07	0.79	1.00	
Denudation rates corrected for Qz content in bedrock (mm/ka) (Reber et al., in review)	-0.22	0.01	-0.04	0.30	0.06	-0.03	-0.17	0.64	0.05	0.54	0.65	-0.11	0.84	0.99	1.00

Table 3: Results of the statistical investigations, illustrated here as correlation matrix values.
The valuess in bold show significant correlation between the grain size data and the morphometric parameters and basins characteristics

	Altitude (m)	*Latitude (DD WGS84)*	*Longitude (DD WGS84)*	***D50 (cm)***	***D84 (cm)***	***D96 (cm)***	***b/a***	*Catchment area (km2)*	*Mean slope (m/m)*	*Distance form the western escarpment (km)*	*Mean annual water discharge (m3/s)*	*Shear stress*	*Sediment flux*	*Denudation rates (mm/ka)*	*Denudation rates corrected for Qz content in bedrock (mm/ka)*
Altitude (m)	**< 0.00001**														
Latitude (DD WGS84)	0.11	**< 0.00001**													
Longitude (DD WGS84)	**0.03**	**< 0.00001**	**< 0.00001**												
D50 (cm)	0.69	1.00	0.96	**< 0.00001**											
D84 (cm)	0.54	0.86	0.89	**< 0.00001**	**< 0.00001**										
D96 (cm)	0.43	0.93	0.93	**0.000172**	**< 0.00001**	**< 0.00001**									
b/a	0.27	**0.007**	**0.003**	0.75	1	0.94	**< 0.00001**								
Catchment area (km2)	0.27	0.60	0.60	0.17	0.48	0.86	0.37	**< 0.00001**							
Mean slope (m/m)	0.31	**0.0002**	**< 0.00001**	0.76	0.66	0.89	**0.01**	0.22	**< 0.00001**						
Distance form the western escarpment (km)	0.15	0.54	0.54	0.11	0.48	0.89	0.22	**< 0.00001**	0.11	**< 0.00001**					
Mean annual water discharge (m3/s) (Reber et al., in press)	0.18	0.89	0.96	0.43	0.82	0.77	0.64	**< 0.00001**	0.31	**< 0.00001**	**< 0.00001**				
Shear stress	**0.04**	0.63	0.54	0.31	0.14	**0.08**	0.83	0.36	0.79	0.31	**0.098**	**< 0.00001**			
Sediment flux	0.31	0.40	0.46	**0.05**	0.46	0.89	0.45	**< 0.00001**	0.29	**< 0.00001**	**< 0.00001**	0.33	**< 0.00001**		
Denudation rates (mm/ka) (Reber et al., in press)	0.31	0.86	0.69	0.13	0.69	1.00	0.75	**0.01**	0.60	**0.027**	**0.008**	0.76	**< 0.00001**	**< 0.00001**	
Denudation rates corrected for Qz content in bedrock (mm/ka) (Reber et al., in press)	0.33	0.96	0.86	0.18	0.79	0.89	0.55	**0.001**	0.82	**0.011**	**0.0014**	0.63	**< 0.00001**	**< 0.00001**	**< 0.00001**

Table 4: Results of the statistical investigations, illustrated here as correlation matrix of the p-values.
The values in bold have a significance level alpha < 0.1